Highly Selective and Scalable Fullerene-Cation-Mediated Synthesis accessing Cyclo[60]fullerenes with 5-Membered-Carbon-Ring and their Application to Perovskite Solar Cells

Hao-Sheng Lin,[1] Il Jeon,*[,1] Yingqian Chen,[2] Xiao-Yu Yang,[3] Takafumi Nakagawa,[1] Shigeo Maruyama,[1,4] Sergei Manzhos,[2,5] and Yutaka Matsuo*[,1,3,6]

[1] Department of Mechanical Engineering, School of Engineering, The University of Tokyo, 7-3-1, Hongo, Bunkyo-ku, Tokyo 113-8656, Japan

[2] Department of Mechanical Engineering, National University of Singapore, Block EA #07-08, 9 Engineering Drive 1, Singapore 117576, Singapore

[3] Hefei National Laboratory for Physical Sciences at the Microscale, University of Science and Technology of China, 96 Jinzhai Road, Hefei, Anhui 230026, P. R. China

[4] Energy NanoEngineering Laboratory, National Institute of Advanced Industrial Science and Technology (AIST), Tsukuba, 305-8564 Japan

[5] Centre Énergie Matériaux Télécommunications, Institut National de la Recherche Scientifique, 1650 boulevard Lionel-Boulet, Varennes QC J3X1S2, Canada

[6] Institute of Materials Innovation, Institutes of Innovation for Future Society, Nagoya University, Furo-cho, Chikusa-ku, Nagoya 464-8603, Japan

ABSTRACT: Cyclo[60]fullerenes are widely used in many applications including photovoltaic devices owing to their high electron affinity and mobility for an organic molecule. However, their synthesis has been limited to certain derivatives with low yields. In this work, a fullerene-cation-mediated synthesis, accessing a new class of 5-membered-carbon-ring cyclo[60]fullerenes with high yields of up to 93% is showcased. This method utilizes aryl[60]fullerene cations, ArC_{60}^{+} as intermediates, which are generated *in situ* by heating the aryl[60]fullerenyl dimers in the presence of $CuBr_2$. In addition, 5-membered-carbon-ring cyclo[60]fullerenes display excellent device applicability when they are used in perovskite solar cells as over-coating layers of electron-transporting layers. A power conversion efficiency of 20.7% is achieved thanks to the favorable energy alignment, optimized substrate design, and electrochemical stability of the 5-membered-carbon-ring fullerenes.

■ INTRODUCTION

Fullerene and its derivatives have attracted much attention owing to their versatile applicability in the fields of photovoltaics, bioscience, and space science.[1-5] In thin-film photovoltaics, cyclo[60]fullerenes have been used as electron acceptors in organic solar cells[6-10] and as electron-transporting layers (ETLs) in perovskite solar cells[11-13]. In particular, cyclo[60]fullerenes as an over-coating layer of metal oxide ETLs have been one of the most exploited applications in perovskite solar cells, demonstrating a dramatic reduction hysteresis and enhancement of the device charge-dynamics.[14-20] With respect to such applications, heterocyclo[60]fullerene,[14-19] which is one of the most abundant types of cyclo[60]fullerene, have shown relatively poor performance compared with full-carbon-ring cyclo[60]fullerenes because of their electrochemical instability.[21-23] Accordingly, cyclo[60]fullerenes with a full-carbon-ring, such as 3-membered-carbon-rings (e.g. $PC_{61}BM$)[18-20,24,25] and 6-membered-carbon-rings (e.g. ICBA, MIF),[7,26-28] have been the preferred choices for the over-coating layers of metal oxide ETLs. Yet, cyclo[60]fullerenes with a 5-membered-carbon-ring, namely indano[60]fullerenes, have never been demonstrated to date.[29-34] This is because the existing synthetic methods exhibit low yields and a limited substrate scope of fullerene derivatives.

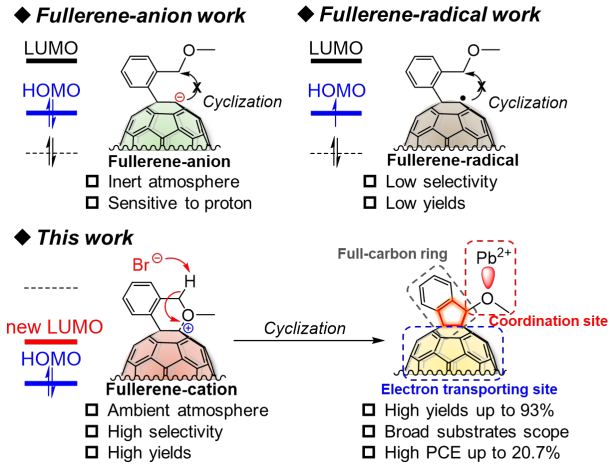

Figure 1. Concept of this work. The newly generated LUMO has unique reactivity, enabling the production of cylclo[60]fullerenes with 5-membered-carbon-ring.

In this work, we report a cyclo[60]fullerene synthesis mediated by fullerene-cation intermediates, which accesses cyclo[60]fullerenes with a 5-membered-carbon-ring in scalable yields. The fullerene-cation-mediated reactions can render more facile and controlled derivatization of fullerenes than conventional fullerene-anion-mediated or fullerene-radical-mediated reactions (**Figure 1**).[35-37] This is because the fullerene-cation-mediated reaction harnesses *in situ*-generated fullerene cations, which are highly reactive due to exceptionally low energy level of the newly formed lowest unoccupied molecular orbitals (LUMOs).[38] Such high reactivity of the intermediates leads to high selectivity, thus a scalable yield with an excellent functional group tolerance. Accordingly, this fullerene-cation-mediated methodology enabled the production of rare fullerenes, indano[60]fullerene derivatives in this work. The synthesis of indano[60]fullerenes showed high yields as expected (the highest *ca.* 93%). The mechanism of this new synthetic route was investigated and discussed as well. Moreover, we explored the device application of indano[60]fullerenes in perovskite solar cells as 3- or 6-membered-carbon-rings[18-20,26-28,39-41] and 5-membered-heteroatom-rings[14-19,42-44] have been widely used in devices. We found that the hydrophobicity,[45-47] solubility, reorganization energy of fullerene,[48-51] and the ability to passivate the perovskite interface[52-53] were crucial in obtaining high power conversion efficiency (PCE). Among different fullerene derivatives synthesized in this work, indano[60]fullerene (**5a**) gave a PCE of 20.7% when used as the over-coating layer in perovskite solar cells. The obtained PCE was higher than 19.0% and 16.5% of the reference devices in which C_{60} and $PC_{61}BM$ were used, respectively. Not only was it, the efficiency of 20.7% stands the highest among the reported fullerene over-coating ETL-based $NH_3CH_3PbI_3$($MAPbI_3$)-used perovskite solar cells.

■ EXPERIMENTAL SECTION

Materials.

Unless otherwise noted, all materials including dry solvents were obtained from commercial suppliers (Adamas-beta, TCI) and used without further purification. C_{60} and $PC_{61}BM$ were purchased from American dye Inc. PbI_2 (99.9985%) and methylammonium iodide (MAI) was purchased from Sigma-Aldrich Inc. Anhydrous *N*,*N*-dimethylformamide (DMF), dimethyl sulfoxide (DMSO), *ortho*-dichlorobenzene (*o*-DCB), and chlorobenzene (CB) were purchased from Alfa Aesar. Spiro-MeOTAD was purchased from Luminescence Technology Corp. (Lumtec).

SnO_2 precursor solution preparation. 27.1 mg $SnCl_2{\cdot}2H_2O$ (Aldrich, >99.995%) white powder was dissolved in 4.0 mL of anhydrous ethanol (TCI), which was filtered by 0.22 μm syringe filter before using.

Fullerene solution preparation. 5.0 mg of fullerene, or FIFs was dissolved in 1.0 mL anhydrous *o*-DCB and then filtered by 0.22 μm syringe filter before using.

$MAPbI_3$ precursor solution preparation. 355 mg of PbI_2, 122 mg of CH_3NH_3I, and 54.7 μL of DMSO (molar ratio 1:1:1) were mixed in 490.5 μL of DMF solution at room temperature with stirring for 1 h. The solution was filtered through a 0.45 μm polytetrafluoroethylene filter prior to use.

Spiro-MeOTAD solution preparation. A solution was prepared by mixing 85.8 mg Spiro-MeOTAD, 19.3 μL of a stock solution of 520 mg mL^{-1} lithium bis(trifluoromethylsulphonyl)-imide in anhydrous acetonitrile, and 33.8 μL of 4-*tert*-butylpyridine in 1.0 mL anhydrous chlorobenzene.

Synthesis of 5-membered-carbon ring fullerenes. Unless otherwise noted, all reactions were performed with dry solvents under an atmosphere of argon in flame-dried glassware with standard vacuum-line techniques.

Synthesis of aryl bromides (1a–g).[54-57] MeOH (20.0 mL) was slowly added to sodium (517.5 mg, 22.5 mmol) at 0°C. After Na completely reacted with MeOH, different functionalized benzyl bromide (15 mmol) was added into the resulting solution at room temperature for 5 hours. Then, the resulting suspension was quenched by 10 mL H_2O and extracted with CH_2Cl_2 (10×3 mL). Combined organic layers were dried by $MgSO_4$, and the solvent was removed under the reduced pressure to give a crude product. The further separation was carried on a silica gel column with n-hexane/ethyl acetate (10/1, v/v) as eluent, producing **1a–g** as a colorless oil.

Synthesis of Grignard reagents (2a–g). An anhydrous tetrahydrofuran (THF) (10.0 mL) solution of aryl bromides **1a–g** (10 mmol) was slowly dropped into polished Mg powder (360.0 mg, 15 mmol) in a trace amount of I_2 as initiator under an argon atmosphere at 0 °C. After vigorously stirred 1 hour, the prepared Grignard solution (**2a–g**) was transferred by Schlenk operation and stocked in a Schlenk bottle. The concentration was confirmed before using through anhydrous titration by using menthol as titrant with a trace amount of 1,10-phenanthroline as indicator under an argon atmosphere.

Synthesis of arylhydro[60]fullerenes ($ArC_{60}H$, 3a–g). C_{60} (300.0 mg, 0.417 mmol) was dissolved in anhydrous *o*-dichlorobenzene (*o*-DCB) (50.0 mL) containing 1,3-dimethyl-2-imidazolidinone (DMI) (1.4 mL, 12.5 mmol) as co-solvent. Then, previous synthesized Grignard reagent (**2a–g**) was added into the solution at 25 °C under an argon atmosphere. After stirring for 15 min, CH_3COOH (0.1 mL, 1.75 mmol) was added to quench the reaction and then the solvent was evaporated in *vacuo*. The residue was dissolved in CS_2 and purified through a silica gel column via CS_2/CH_2Cl_2 as the eluent to afford product **3a–g**.

Synthesis of aryl[60]fullerenyl dimers (ArC_{60}–$C_{60}Ar$, 4a–g). Above synthesized monoadducts (**3a–g**) (0.048 mmol) was dissolved in 5.0 mL anhydrous *o*-DCB solution. Then, a solution of *t*-BuOK (58 μL, 0.058 mmol, 1M) in THF was added and vigorously stirred at room temperature under an argon atmosphere for 15 min. Subsequently, *N*-bromosuccinimide (NBS) (34.2 mg, 0.192 mmol) was added. The reaction mixture was vigorously stirred for 12 hours at room temperature under the argon atmosphere. Then the resulting brownish suspension was quenched by 1.0 mL H_2O and an excess amount of MeOH was added to precipitate the crude product. Finally, titled dimers (**4a–g**) were collected as a residue by filtration without necessities of further purifications.

Synthesis of titled FIFs (5a–g). 0.030 mmol of dimers (**4a–g**) was dissolved in 10.0 mL of anhydrous *o*-DCB solution in the presence of $CuBr_2$ (26.8 mg, 0.120 mmol) as oxidant. After being vigorously stirred at 100 °C for 3 h, the resulting mixture was directly filtered through a silica gel plug to remove insoluble salt and then evaporated in *vacuo* to remove the solvent. Next, the residue was further separated on a silica gel column with CS_2 as eluent to afford products **5a–g**.

Molecular characterization. All NMR spectra were taken at 400 MHz (Bruker AVANCE III 400 spectrometer), 500 MHz (Bruker AVANCE III 500 spectrometer) or 600 MHz (Bruker AVANCE III 600 spectrometer). Unless otherwise specified, all the NMR spectra were recorded in parts per million (ppm, scale) with the proton of $CDCl_3$ (7.260 ppm) or the proton of 1,1,2,2-tetrachloroethane-d_2 (TCE-d_2) (6.000 ppm) for ^1H NMR and carbon of $CDCl_3$ (77.16 ppm) or carbon of TCE-d_2 (73.78 ppm) for ^{13}C NMR as internal reference, respectively. The data were presented as following order: chemical shift, multiplicity (s = singlet, d = doublet, t = triplet, hept = heptet, m = multiplet and/or multiplet resonances), coupling constant in hertz (Hz), and signal area integration in natural numbers, assignment (*italic*). High-resolution mass spectra (HRMS) were obtained by MALDI using a time-of-flight mass analyzer on a Bruker Ultra exTOF/TOF spectrometer. Potentials in V *vs* a ferrocene/ferrocenium (Fc/Fc^+) couple were recorded by cyclic voltammetry in an *o*-DCB solution containing $Bu_4N^+CF_3SO_2N^-$ (0.1 M) as supporting electrolyte at 25 °C with a scan rate of 0.05 V/s. Platinum disk, platinum wire, and Ag/Ag^+ electrodes were used as the working, counter, and reference electrodes, respectively. The valence band and Fermi levels measurements were performed using Riken Keiki PYS-A AC-2 and Kelvin probe spectroscopy in the air (ESA), respectively

Device fabrication. Indium-doped tin oxide (ITO) patterned glass substrates were cleaned and sonicated with detergent, distilled water, acetone and isopropanol in an ultrasonic bath for 15 min, respectively. Next, the cleaned ITO substrates were treated with UV/O_3 for 15 min. Subsequently, 25 μL of SnO_2 precursor solution was spin-coated on the cleaned ITO substrate at 3000 rpm for 30 s, which was annealed at 150 °C for 45 min. After cooling down to room temperature, the spin-coating process was repeated one more time followed by annealing at 180 °C for 1 h. Then, the SnO_2 coated ITO glass was further treated with UV/O_3 for 15 min before spin-coating of fullerene solution. 25 μL of fullerene solution was spin-coated on the top of the SnO_2 layer at 4000 rpm for 30 s. Next, 25 μL of perovskite precursor solution was spin-coated on the fullerene layer at 4000 rpm for 30 s, with slowly dropping 0.5 mL of anhydrous diethyl ether onto the substrate 10 s after the start of the spin-coating process, followed up with annealing at 100°C for 10 min. The hole transporting layer was spin-coated from the 20 μL of Spiro-MeOTAD solution at 4000 rpm for 20 s. Finally, a 70-nm-thick of Au anode was fabricated by thermal deposition at a constant evaporation rate of 0.05 nm s^{-1} under pressure of 10^{-6} Torr.

Photovoltaic characterization and measurement. The current density vs voltage (*J*–*V*) characteristics were measured using a software-controlled source meter (Keithley 2400 SourceMeter) under dark conditions and the simulated sunlight irradiation of 1 sun (AM 1.5G; 100 mW cm^{-2}) using a solar simulator (EMS-35AAA, Ushio Spax Inc.) with an Ushio Xe short arc lamp 500. The source meter was calibrated using a silicon diode (BS-520BK, Bunkokeiki). When evaluating, devices were masked with a black aperture to set the active area of the device to 0.1 cm^2. Shimadzu IRAffinity-1s was used for the Fourier transform infrared spectroscopy (FT-IR) measurement. External quantum efficiency (EQE) spectra were measured using machine spectrometer with a wavelength ranging from 300 nm to 850 nm. Steady-state PL spectra were measured using a photoluminescence (PL) spectrometer (JASCO Spectrofluorometer FP-8300) with Xenon as the excitation source (excitation at 560 nm). The detected emission wavelength of the steady-state PL was from 675 nm to 875 nm. The water contact angle measurements were performed using a contact angle meter (DMo-501, Kyowa Interface Science Co., Ltd.). Scanning electron microscopy (SEM) measurements were carried out on an S-4800 scanning electron microscopy (Hitachi).

Space-charge-limited current (SCLC) measurement. The structure of the ETL-only device was ITO/Fullerenes(30 nm)/Al(80 nm). The mobility was determined by fitting the dark current to a model of a single-carrier SCLC, which is described by the equation, $J_{SCLC} = 9\varepsilon_0\varepsilon_r\mu V^2/8L^3$, where J_{SCLC} is the current density, μ is the mobility, ε_0 is the permittivity of free space, ε_r is the relative permittivity of the material, *L* is the thickness of the fullerenes layer, and *V* is the effective voltage. The thicknesses of the fullerene layer were measured using cross-sectional SEM images. Over-coating fullerene on SnO_2 ETL layers failed to give mobility data that can differentiate between the samples, due to the low thickness of the over-coating fullerene layers. Therefore, we measured a single layer of fullerene by using CS_2 (25 mg mL^{-1}) as the solvent. The experimental dark current density was measured under an applied voltage swept from 0 to –5 V.

Trap density and trap-filling limit voltage measurement.[58-61] Trap density (n_t) and trap-filling limit voltage (V_{TFL}) were measured based on SCLC using charge carrier only devices with a structure of ITO/SnO_2(30 nm)/Fullerenes(5 nm)/$MAPbI_3$(400 nm)/$PC_{61}BM$(30 nm)/Au(60 nm). The n_t and V_{TFL} values are calculated from the equation, $V_{TFL} = n_t ed^2/2\varepsilon_0\varepsilon_r$, where *e* is electric charge (1.602×10^{-19} V/m), *d* is thickness of the active layer, ε_0 is the vacuum permittivity (8.85×10^{-14} F/cm) and ε_r is the relative dielectric constant taken as 46.9.[59] The experimental dark current density was measured under an applied voltage swept from 0 to –5 V.

■ RESULTS AND DISCCUSION

Arylhydro[60]fullerenes ($ArC_{60}H$, **3a**–**g**), the precursor of aryl[60]fullerenyl dimers, were prepared by nucleophilic addition of functionalized Grignard reagents (**2a**–**g**) in isolated yields up to 95% (**Table S1**).[62] It is worth noting that 1,3-dimethyl-2-imidazolidinone (DMI) was introduced as co-solvent instead of dimethyl sulfoxide (DMSO) or *N*,*N*-dimethylformamide (DMF) to obtain arylhydro[60]fullerenes in high selectivity. DMI has a planar configuration unlike DMSO or DMF, which means that DMI can form more stable coordination to the Mg^{2+}, prohibiting a multi-addition. Next, the key precursors, aryl[60]fullerenyl dimers (ArC_{60}–$C_{60}Ar$, **4a**–**g**) were synthesized using *N*-bromosuccinimide (NBS) in a high stoichiometric yield. Such high yield comes from the fact that NBS functions as an oxidant in the single-electron oxidation of arylfullerenyl anions (ArC_{60}^-), which is produced by the deprotonation of $C_{60}ArH$ in the presence of ^{t}BuOK (**Table S2**). Therefore, ArC_{60}–$C_{60}Ar$ did not require a laborious further purification, for example, chromatography. Then, the reaction conditions were optimized to heating aryl[60]fullerenyl dimer (**4a**) at 100 °C in the presence of 4.0 equiv. $CuBr_2$ under an ambient atmosphere for 3.0 hours (**Table S3**). The optimized condition produced indano[60]fullerene (**5a**) with a yield of 93% (**Table 1, Entry 1**). Another fullerene derivative, methyl substituted indano[60]fullerene (**5b**) was synthesized and isolated in a yield of 90% (**Table 1, Entry 2**). To investigate the electronegativity influence of the substituents on fullerenes, electron-donating methoxyl- and electron-withdrawing fluoro moiety-attached fullerene derivatives were synthesized. The corresponding derivatives **5c** and **5d** gave yields of 86% and 73%, respectively (**Table 1, Entry 3** and **4**). Although fullerenes with electron-donating groups, in general, give good yields, the yield of **5c** was lower than that of the non-substituted substrate, **5a**. This can be attributed to the poor

solubility of methoxy-substituted fullerene derivatives.[63-64] In addition, fullerene derivatives with long carbon chains as the R^2 functional group were synthesized, because long carbon chains on fullerenes are known to enhance the solubility.[65-67] Hexyl substituted derivative (**5e**) and 2-ethylhexyl substituted derivative (**5f**) were produced in yields of 56% and 41%, respectively (**Table 1, Entry 5** and **6**). Expectedly, **5e** and **5f** possessed high solubility that they could be dissolved in *o*-DCB with saturated concentrations of 22.8 mg mL^{-1} and 28.6 mg mL^{-1} at 25 °C, respectively. Notably, the fullerene-cation-mediated cyclo[60]fullerene synthetic protocol can be extended to produce 6-membered ring derivatives. The 6-membered ring fullerene derivative (**5g**) was synthesized for comparison and its yield was 89% (**Table 1, Entry 7**). It should be highlighted that this fullerene-cation-mediated cyclo[60]fullerene showed a total yield of up to 87%, which is a scalable yield.

Table 1. Fullerene-cation-mediated intramolecular cyclization with versatile substrates[a]

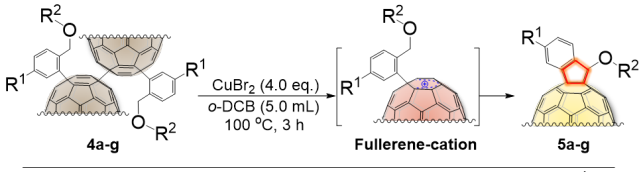

Entry	R_1	R_2	Products 5	Yield (%)[b]
1	H-	CH_3-	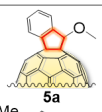 5a	93
2	CH_3-	CH_3-	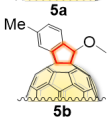 5b	90
3	CH_3O-	CH_3-	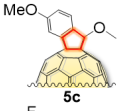 5c	86
4	F-	CH_3-	 5d	73
5	H-	$CH_3(CH_2)_5$-	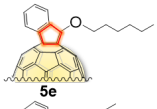 5e	56
6	H-	$CH_3(CH_2)_3CHCH_2$- CH_2CH_3	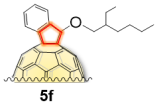 5f	41
7	H-	CH_3-	 5g	89

[a] Unless otherwise specified, all reactions were performed with 0.03 mmol of **4a–g** and 0.12 mmol of $CuBr_2$ in 5.0 mL of *ortho*-dichlorobenzene (*o*-DCB) solution at 100 °C for 3.0 h under an ambient atmosphere. [b] Isolated yield.

Additional experiments provide an insight into the reaction mechanism. Two control experiments were conducted to explore the possibility of intramolecular cyclization through a radical pathway or cationic mechanism. When aryl[60]fullerenyl dimer **4a** was heated to 100 °C in the absence of $CuBr_2$, the reaction produced insoluble fullerene aggregations instead of the target molecule **5a** (**Figure S1b**). Similarly, when the reaction was conducted in the presence of $CuBr_2$ and 2,2,6,6-tetramethylpiperidine-1-oxyl (TEMPO), the latter of which is a radical scavenger, there was no trace of **5a** (**Figure S1c**). These additional experiments conclusively demonstrate that the fullerene-cation-intermediate is generated by the oxidation of fullerenyl radical in the presence of Cu[II]. Therefore, a plausible mechanism is proposed like the following (**Scheme 1**): First, the radical intermediate **I** is generated through thermolysis upon heating aryl[60]fullerenyl dimers **4**. Then, the radical intermediate **I** is further oxidized by Cu[II] to form the key aryl[60]fullerenyl cation **II.** Finally, **II** undergoes an intramolecular cyclization triggered by the bromide with loss of one proton, producing the target molecule cyclo[60]fullerenes **5**.

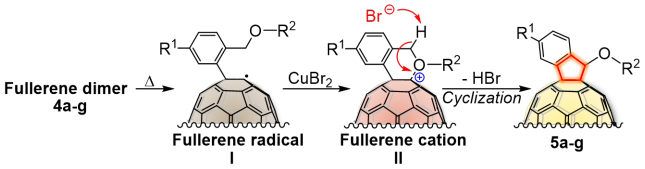

Scheme 1. Plausible reaction mechanism of the fullerene-cation-mediated intramolecular cyclization reaction.

Subsequently, we investigated the applicability of the indano[60]fullerenes to perovskite solar cells. Energy levels are important for the ETL application in photovoltaics.[68-70] Therefore, we conducted the cyclic voltammograms (CVs) and photoelectron yield spectroscopy (PYS) along with the Kelvin probe measurement on the cyclo[60]fullerene derivatives, **5a–g**, to evaluate the LUMO levels, the highest occupied molecular orbital (HOMO) levels, and the Fermi levels, respectively. The CV data show that all the derivatives possess slightly higher LUMO levels to C_{60}, which is a commonly used ETL for perovskite solar cells (**Figure S2**). It should be mentioned that **5g**, which has a 6-membered ring, manifested an irreversible peak at its third reductive wave, which clearly demonstrates poor electrochemical stability compared with the other fullerene derivatives containing a 5-membered ring. Density functional theory (DFT) also predicts that the LUMOs of the selected fullerene derivatives have similar energies (**Figure S3** and **S4; Table S4**). The PYS and the Kelvin probe data in **Table S4** show that all the fullerene derivatives have comparable HOMO levels and Fermi levels that they are energetically compatible as the ETL.

Table 2. Photovoltaic parameters of the normal-type perovskite solar cells using fullerenes as the over-coating layer of ETL under 1 sun (AM 1.5 G, 100 mW cm^{-2}). Average values with standard deviation are obtained from 20 devices in the same batch and the statistical analyses provided in **Figure S12**.

Entry	Fullerenes	J_{SC} (mA cm^{-2})	V_{OC} (V)	FF	R_S (Ω cm^2)	R_{SH} (Ω cm^2)	PCE_{best}	$PCE_{average}$	Hysteresis Index[71]

1	–	22.8 ±0.2	1.070 ±0.004	0.73 ±0.01	48.2	$1.46x10^5$	18.6%	18.1 ±0.5%	0.073
2	C_{60}	23.2 ±0.3	1.070 ±0.005	0.75 ±0.02	34.2	$7.58x10^5$	19.0%	18.6 ±0.4%	0.056
3	$PC_{61}BM$	23.5 ±0.3	1.040 ±0.005	0.65 ±0.01	44.1	$5.21x10^5$	16.5%	16.1 ±0.3%	0.132
4	**5a**	**23.7 ±0.2**	**1.089 ±0.003**	**0.78 ±0.01**	**29.7**	**$8.03x10^5$**	**20.7%**	**20.5 ±0.2%**	**0.038**
5	**5b**	22.3 ±0.3	1.064 ±0.003	0.75 ±0.01	46.9	$1.09x10^5$	18.5%	18.0 ±0.5%	0.115
6	**5d**	22.8 ±0.2	1.070 ±0.004	0.71 ±0.01	52.8	$8.62x10^4$	18.6%	18.1 ±0.5%	0.114
7	**5e**	23.2 ±0.3	1.074 ±0.005	0.74 ±0.01	32.8	$1.38x10^5$	18.7%	18.5 ±0.2%	0.065
8	**5f**	23.6 ±0.2	1.070 ±0.004	0.73 ±0.02	30.9	$3.35x10^5$	18.8%	18.4 ±0.4%	0.067
9	**5g**	23.0 ±0.2	1.058 ±0.004	0.71 ±0.02	53.2	$2.65x10^5$	17.6%	17.2 ±0.4%	0.107

We fabricated normal-type perovskite solar cells, in which the fullerenes over-coat SnO_2 (**Figure 2a, S5, S6,** and **S7; Table S5**). Perovskite solar cells with **5a** as the over-coating layer showed the highest PCE of 20.7% with a short-circuit current density (J_{SC}) of 23.8 mA cm^{-2}, an open-circuit voltage (V_{OC}) of 1.09 V, and a fill factor (FF) of 0.79 (**Figure 2b; Table 2: Entry 4**). The PCE was significantly higher than those of the reference devices without fullerene (18.6%), with C_{60} (19.0%), and $PC_{61}BM$ (16.5%) (**Figure 2b; Table 2: Entry 1, 2,** and **3**). Such higher performance can be attributed to the higher LUMO level of **5a** (58-π system) compared with C_{60} (60-π system) (**Figure S2**) and a passivation effect of the ether addend (**Figure 2c** and **S8**). In addition, the photoluminescence (PL) measurement showed a greater PL quenching of $MAPbI_3$ on a **5a** film than that on a C_{60} film (**Figure S9**). Moreover, the PL peak of $MAPbI_3$ on the **5a** film was more blue-shifted than that on the C_{60} film, indicating more reduced trap states at the interface between the **5a** film and $MAPbI_3$.[50] Furthermore, the space-charge limited current (SCLC) measurement was carried out to compare **5a** and C_{60} films, respectively (**Figure S10** and **Table S6**). The **5a** film possessed a similar electron mobility (4.06×10^{-6} cm^2Vs^{-1}) compared with C_{60} (7.25×10^{-6} cm^2 Vs^{-1}). Additional SCLC experiments using charge only devices were carried out to compare the trap density (n_t) and trap-filling limit voltage (V_{TFL}) of the **5a**- and C_{60}- applied devices, respectively (**Figure S11** and **Table S7**). The **5a**- applied device showed lower V_{TFL} (0.31 V) and n_t (1.00×10^{16} cm^{-3}) compared with V_{TFL} (0.47 V) and n_t (1.52×10^{16} cm^{-3}) of the C_{60}-applied device. Accordingly, the higher FF of the **5a**-based devices is not from the electron mobility, rather from the mentioned reduced surface trap-sites and the higher LUMO level of **5a**. The effective passivation meant that the perovskite crystal grain size was affected by this. The average grain size of perovskite film on the SnO_2/**5a** is larger than that of the bare SnO_2 according to the SEM images shown in **Figure S12**. It can be deduced that the passivation effect of **5a** retarded the crystal growth, which is also reflected by the higher J_{SC} value of the **5a**-based devices compared with the reference.[70] To ascertain this, X-ray diffraction (XRD) spectroscopy was conducted (**Figure S13** and **Table S8**). The tetragonal phase of perovskite films was depicted with a dominant peak (110) at 14.0°. The full-width at half-maximum (FWHM) of the (110) peaks was calculated through the Debye-Scherrer equation to estimate the crystal grain size.[72] The bare SnO_2/$MAPbI_3$ film, the SnO_2/C_{60}/$MAPbI_3$ film, and the SnO_2/**5a**/$MAPbI_3$ film showed (110) peaks with FWHM values of 0.467, 0.463, and 0.419, respectively, indicating that the crystal grain size of the SnO_2/**5a**/$MAPbI_3$ films is the largest. Moreover, the intensity ratio of the (110) peak to the (220) peak demonstrates the growth of the (110)-oriented grains, which indicates the favorable hole injection from the perovskite to hole-transporting layer.[73-75] The perovskite film on a SnO_2/**5a** film presented the greatest ratio of 1.78 compared with 1.63 and 1.67 of the perovskite films on SnO_2 and SnO_2/C_{60}, respectively.

However, not all the cyclo[60]fullerene derivatives gave good performance. Spin-coating **5b** on SnO_2 resulted in poor film coverage (**Figure S14** and **S15; Table 2: Entry 5**). Poor coverage led to the formation of pinholes in the ETL as evidenced by low V_{OC} and larger hysteresis of the *J*–*V* curves (**Figure S6**).[76] Besides, despite **5b** having a similar structure to **5a**, it possessed a lower reorganization energy, λ, which accounts for the low performance due to a decreased charge separation rate (**Table S9**). In the case of **5c**, the fullerene could not be coated at all, due to the intrinsic low solubility as mentioned above. The **5d** film had a problem of being too hydrophobic, because of the attached F atom. As a result, perovskite films could not be coated uniformly on the fullerene layer (**Figure S6** and **S15; Table 2, Entry 6**). Although **5e**- and **5f**-used devices exhibited high J_{SC} and V_{OC}, their FF values were also not as high as that of the **5a**-used devices. This is because the ether group on **5e** and **5f** could not passivate the perovskite interface due probably to the steric effect of the long alkyl chains (**Figure 2e and 2f; Table 2: Entry 7** and **10**). Additionally, the reorganization energy of **5f** was lower than that of **5a** (**Figure S16** and **Table S9**). **5g** has a 6-membered-carbon-ring as opposed to the 5-membered-carbon-rings of other fullerene derivatives tested in this work. The device performance of the **5g**-based perovskite solar cells was not as high as the other fullerene-based perovskite solar cells (**Figure S7** and **S16; Table 2: Entry 9**). We ascribe this to the hydrophobicity and subsequent poor coverage of $MAPbI_3$ (**Figure S14** and **S15**), less favorable effective driving force and reorganization energy of **5g** (**Table S9**). Further, the CV of **5g** showed an irreversible peak at its third redox potential, which suggests a possible cleavage of the 6-membered ring on **5g** under an operating condition. This points to the fact that cyclo[60]fullerenes with a 6-membered-ring are not feasible for the solar cell application, which is probably why there has not been a report on device application of cyclo[60]fullerenes with a 6-membered-ring. It is important to emphasize that the best PCE of 20.7% obtained from the **5a**-based perovskite solar cells is highly reproducible (**Figure S17**) and stands by far the highest among the reported fullerene over-coating ETL-based $MAPbI_3$-used perovskite solar cells (**Figure S18** and **Table S10**).[14-20,24,25,77-87]

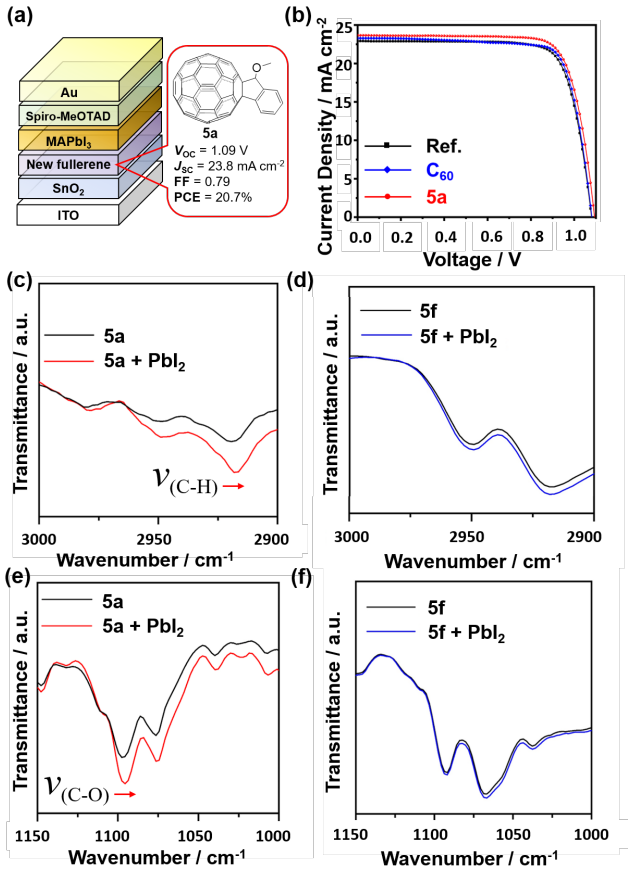

Figure 2. (a) Illustration of normal-type perovskite solar cells structure used in this work with fullerenes as over-coating layers. Cross-sectional SEM observations provided in **Figure S7**. (b) *J*–*V* curves of selected examples: reference (black line), $PC_{61}BM$ (blue line), **5a** (red line). Reflective Fourier transform infrared (FTIR) spectra of cyclo[60]fullerenes **5a** (red line) for (c) $\nu_{(C-H)}$ and (d) $\nu_{(C-O)}$, **5f** (blue line) for (e) $\nu_{(C-H)}$ and (f) $\nu_{(C-O)}$ with and without the presence of PbI_2.

■ CONCLUSIONS

In summary, we report a new synthetic strategy of cyclo[60]fullerenes using fullerene cation intermediates, which give by far greater yields than the conventional approach. We revealed the mechanism of how the *in situ* aryl[60]fullerene cations function as intermediates that enhance the selectivity of the reaction and enables a broad substrate scope. Using the new synthetic method, various designs of cyclo[60]fullerenes with a 5-membered-ring were synthesized. Their device application as the ETL over-coating layer in perovskite solar cells was demonstrated as well, which resulted in the extremely high PCE compared with the values reported in the literatures. We conclude that the design of fullerene derivatives with the balance of the solubility, high reorganization energy, and ability to passivate the active layer interface is equally as important as the conventional approaches of tuning the LUMO levels for the ETL application in perovskite solar cells. We believe that this communication will provide a better understanding of the fullerene cation chemistry as well as the fullerene design for device applications.

■ ASSOCIATED CONTENT

Supporting Information

The Supporting Information includes experimental details, reaction mechanism, morphology investigation, computational study, ^{1}H NMR, ^{13}C NMR, UV-Vis spectroscopy, PL spectroscopy, SCLC measurement and device performance tests. The Supporting Information is available free of charge on the ACS Publications website at DOI:

■ AUTHOR INFORMATION

Corresponding Author

*E-mail: il.jeon@spc.oxon.org (I.J.).
*E-mail: matsuo@photon.t.u-tokyo.ac.jp (Y.M.)

Notes

The authors declare no competing financial interests.

■ ACKNOWLEDGMENT

We gratefully acknowledge Japan Society for the Promotion of Science (JSPS) KAKENHI Grant Numbers JP15H05760, JP16H02285, JP17H06609, and JP19K15669, the Research and Education Consortium for Innovation of Advanced Integrated Science by Japan Science and Technology (JST), and Yashima Environment Technology Foundation for financial support.

■ REFERENCES

(1) Mishra, A.; Bäuerle, P. Small molecule organic semiconductors on the move: promises for future solar energy technology. *Angew. Chem. Int. Ed.* **2012**, *51*, 2020-2067.
(2) Lai, Y.-Y.; Cheng, Y.-J.; Hsu, C.-S. Applications of functional fullerene materials in polymer solar cells. *Energy Environ. Sci.* **2014**, *7*, 1866-1883.
(3) Campbell, E. K.; Holz, M.; Gerlich, D.; Maier, J. P. Laboratory confirmation of C_{60}^+ as the carrier of two diffuse interstellar bands. *Nature* **2015**, *523*, 322-323.
(4) Martinez, Z. S.; Castro, E.; Seong, C.-S.; Cerón, M.R.; Echegoyen, L.; Llano, M. Fullerene derivatives strongly inhibit HIV-1 replication by affecting virus maturation without impairing protease activity. *Antimcrob. Agents and Chemother*. **2016**, *60*, 5731-5741.
(5) Maier, J. P.; Campbell, E. K. Fullerenes in space. *Angew. Chem. Int. Ed.* **2017**, *56*, 4920-4929.
(6) Zhao, G.; He, Y.; Li, Y. 6.5% Efficiency of polymer solar cells based on poly(3-hexylthiophene) and indene-C_{60} bisadduct by device optimization. *Adv. Mater.* **2010**, *22*, 4355-4358.
(7) Matsuo, Y.; Kawai, J.; Inada, H.; Nakagawa, T.; Ota, H.; Otsubo, S.; Nakamura, E. Addition of dihydromethano group to fullerenes to improve the performance of bulk heterojunction organic solar cells. *Adv. Mater.* **2013**, *25*, 6266-6269.
(8) Chen, J.-D.; Cui, C.; Li, Y.-Q.; Zhou, L.; Ou, Q.-D.; Li, C.; Li, Y.; Tang, J.-X. Single-junction polymer solar cells exceeding 10% power conversion efficiency. *Adv. Mater.* **2015**, *27*, 1035-1041.
(9) Jeon, I.; Delacou, C.; Nakagawa, T.; Matsuo, Y. Enhancement of open-circuit voltage by using the 58-π silylmethyl fullerenes in small-molecule organic solar cells. *Chem. Asian J.* **2016**, *11*, 1268-1272.
(10) Jeon, I.; Sakai, R.; Seo, S.; Morse, G. E.; Ueno, H.; Nakagawa, T.; Qian, Y.; Maruyama, S.; Matsuo, Y. Engineering high-performance and air-stable PBTZT-stat-BDTT-8: $PC_{61}BM/PC_{71}BM$ organic solar cells. *J. Mater. Chem. A* **2018**, *6*, 5746-5751.
(11) Castro, E.; Murillo, J.; Fernandez-Delgado, O.; Echegoyen, L. Progress in fullerene-based hybrid perovskite solar cells. *J. Mater. Chem. C* **2018**, *6*, 2635-2651.
(12) Jeon, I.; Ueno, H.; Seo, S.; Aitola, K.; Nishikubo, R.; Saeki, A.; Okada, H.; Boschloo, G.; Maruyama, S.; Matsuo, Y. Lithium-ion endohedral fullerene ($Li^+@C_{60}$) dopants in stable perovskite solar cells induce instant doping and anti-oxidation. *Angew. Chem. Int. Ed.* **2018**, *57*, 4607-4611.

(13) Chiang, C.-H.; Wu, C.-G. Bulk heterojunction perovskite-PCBM solar cells with high fill factor. *Nature Photonics*, **2016**, *10*, 196-200.

(14) Abrusci, A.; Stranks, S. D.; Docampo, P.; Yip, H.-L.; Jen, A. K.-Y.; Snaith, H. J. High-performance perovskite-polymer hybrid solar cells via electronic coupling with fullerene monolayers. *Nano Lett.* **2013**, *13*, 3124-3128.

(15) Wojciechowski, K.; Stranks, S. D.; Abate, A.; Sadoughi, G.; Sadhanala, A.; Kopidakis, N.; Rumbles, G.; Li, C.-Z. R.; Friend, H.; Jen, A. K.-Y.; Snaith, H. J. Heterojunction modification for highly efficient organic–inorganic perovskite solar cells. *ACS Nano* **2014**, *8*, 12701-12709.

(16) Wang, C., Zhao, D. C.; Grice, R.; Liao, W.; Yu, Y.; Cimaroli, A.; Shrestha, N.; Roland, P. J.; Chen, J.; Yu, Z.; Liu, P.; Cheng, N.; Ellingson, R. J.; Zhao, X.; Yan, Y. Low-temperature plasma-enhanced atomic layer deposition of tin oxide electron selective layers for highly efficient planar perovskite solar cells. *J. Mater. Chem. A* **2016**, *4*, 12080-12087.

(17) Liu, X.; Tsai, K.-W.; Zhu, Z.; Sun, Y.; Chueh, C.-C.; Jen, A. K.-Y. A Low-temperature, solution processable tin oxide electron-transporting layer prepared by the dual-fuel combustion method for efficient perovskite solar cells. *Adv. Mater. Interfaces* **2016**, *3*, 1600122.

(18) Kim, J.; Kim, G.; Kim, T. K.; Kwon, S.; Back, H.; Lee, J.; Lee, S. H.; Kang, H.; Lee, K. Efficient planar-heterojunction perovskite solar cells achieved via interfacial modification of a sol-gel ZnO electron collection layer. *J. Mater. Chem. A* **2014**, *2*, 17291-17296.

(19) Tao, C.; Neutzner, S.; Colella, L.; Marras, S.; Kandada, A. R. S.; Gandini, M.; Bastiani, M. D.; Pace, G.; Manna, L.; Caironi, M.; Bertarelli, C.; Petrozza, A. 17.6% stabilized efficiency in low-temperature processed planar perovskite solar cells. *Energy Environ. Sci.* **2015**, *8*, 2365-2370.

(20) Li, Y.; Zhao, Y.; Chen, Q.; Yang, Y. (M.); Liu, Y.; Hong, Z.; Liu, Z.; Hsieh, Y.-T.; Meng, L.; Li, Y.; Yang, Y. Multifunctional fullerene derivative for interface engineering in perovskite solar cells. *J. Am. Chem. Soc.* **2015**, *137*, 15540-15547.

(21) Yang, W.-W.; Li, Z.-J.; Li, F.-F.; Gao, X. Electrochemical and H/D-labeling study of oxazolino[60]fullerene rearrangement. *J. Org. Chem.* **2011**, *76*, 1384-1389.

(22) Xiao, Y.; Zhu, S.-E.; Liu, D.-J.; Suzuki, M.; Lu, X.; Wang, G.-W. Regioselective electrosynthesis of rare 1,2,3,16-functionalized [60]fullerene derivatives. *Angew. Chem. Int. Ed.* **2014**, *53*, 3006-3010.

(23) Lin, H.-S.; Matsuo, Y.; Wang, J.-J.; Wang, G.-W. Regioselective acylation and carboxylation of [60]fulleroindoline via electrochemical synthesis. *Org. Chem. Front.* **2017**, *4*, 603-607.

(24) Xiao,W. Ke, C.; Wang, C.; Saparov, B.; Duan, H.-S.; Zhao, D.; Xiao, Z.; Schulz, P.; Harvey, S. P.; Liao, W.; Meng, W.; Yu, Y.; Cimaroli, A. J.; Jiang, C.-S.; Zhu, K.; Al-Jassim, M.; Fang, G.; Mitzi, D. B.; Yan, Y. Employing lead thiocyanate additive to reduce the hysteresis and boost the fill factor of planar perovskite solar cells. *Adv. Mater.* **2016**, *28*, 5214-5221.

(25) Liu, K.; Chen, S.; Wu, J.; Zhang, H.; Qin, M.; Lu, X.; Tu, Y.; Meng, Q.; Zhan, X. Fullerene derivative anchored SnO_2 for high-performance perovskite solar cells. *Energy Environ. Sci.* **2018**, *11*, 3463-3471.

(26) He, Y.; Chen, H.-Y.; Hou, J.; Li, Y. Indene–C_{60} bisadduct: a new acceptor for high-performance polymer solar cells. *J. Am. Chem. Soc.* **2010**, *132*, 1377-1382.

(27) Gil-Escrig, L.; Momblona, C.; Sessolo, M.; Bolink, H. J. Fullerene imposed high open-circuit voltage in efficient perovskite based solar cells. *J. Mater. Chem. A* **2016**, *4*, 3667-3672.

(28) Xue, Q.; Bai, Y.; Liu, M.; Xia, R.; Chen, Z.; Hu, Z.; Jiang, X.-F.; Huang, F.; Yang, S.; Matsuo, Y.; Yip, H.-L.; Cao, Y. Dual interfacial modifications enable high performance semitransparent perovskite solar cells with large open circuit voltage and fill factor. *Adv. Energy Mater.* **2017**, *7*, 1602333.

(29) Bingel, C. Cyclopropanierung von fullerenen. *Chem. Ber.* **1993**, *126*, 1957-1959.

(30) Maggini, M.; Scorrano, G.; Prato, M. Addition of azomethine ylides to C_{60}: synthesis, characterization, and functionalization of fullerene pyrrolidines. *J. Am. Chem. Soc.* **1993**, *115*, 9798-9799.

(31) Matsuo, Y.; Nakamura, E. Selective multiaddition of organocopper reagents to fullerenes. *Chem. Rev.* **2008**, *108*, 3016-3028.

(32) Guldi, D. M.; lllescas, B. M.; Atienza, C. M.; Wielopolski, M.; Martín, N. Fullerene for organic electronics. *Chem. Soc. Rev.* **2009**, *38*, 1587-1597.

(33) Liu, T.-X.; Li, F.-B.; Wang, G.-W. Synthesis of [60]fullerene-fused tetrahydronaphthalene and indane derivatives via a pathway switched by aluminum chloride. *Org. Lett.* **2011**, *13*, 6130-6133.

(34) Su, Y.-T.; Wang, G.-W. $FeCl_3$-mediated cyclization of [60]fullerene with N-benzhydryl sulfonamides under high-speed vibration milling conditions. *Org. Lett.* **2013**, *15*, 3408-3411.

(35) Iwashita, A.; Matsuo, Y.; Nakamura, E. $AlCl_3$-mediated mono-, di-, and trihydroarylation of [60]fullerene. *Angew, Chem. Int. Ed.* **2007**, *46*, 3513-3516.

(36) Matsuo,Y.; Ogumi, K.; Zhang, Y.; Okada, H.; Nakagawa, T.; Ueno, H.; Gocho, A.; Nakamura, E. Fullerene cation-mediated demethylation/cyclization to give 5-and 7-membered cyclo[60] fullerene derivatives. *J. Mater. Chem. A* **2017**, *5*, 2774-2783.

(37) Yang, X.-Y.; Lin, H.-S.; Jeon, I.; Matsuo, Y. Fullerene-cation-mediated noble-metal-free direct introduction of functionalized aryl groups onto [60]fullerene. *Org. Lett.* **2018**, *20*, 3372-3376.

(38) Lin, H.-S.; Matsuo, Y. Functionalization of [60]fullerene through fullerene cation intermediates. *Chem. Comm.* **2018**, *54*, 11244-11259.

(39) Xing, Y.; Sun, C.; Yip, H. L.; Bazan, G. C.; Huang, F.; Cao, Y. New fullerene design enables efficient passivation of surface traps in high performance p-i-n heterojunction perovskite solar cell. *Nano Energy* **2016**, *26*, 7-15.

(40) Meng, X.; Bai, Y.; Xiao, S.; Zhang, T.; Hu, C.; Yang, Y.; Zheng, X.; Yang, S. Designing new fullerene derivatives as electron transporting materials for efficient perovskite solar cells with improved moisture resistance. *Nano Energy* **2016**, *30*, 341-346.

(41) Heo, J. H.; Han, H. J.; Kim, D.; Ahn, T. K.; Im, S. H. Hysteresis-less inverted $CH_3NH_3PbI_3$ planar perovskite hybrid solar cells with 18.1% power conversion efficiency. *Energy Environ. Sci.* **2015**, *8*, 1602-1608.

(42) Zhu, Z.; Chueh, C.-C.; Lin, F.; Jen, A. K. Y. Enhanced ambient stability of efficient perovskite solar cells by employing a modified fullerene cathode interlayer. *Adv. Sci.* **2016**, *3*, 1600027.

(43) Watson, B. L.; Rolston, N.; Bush, K. A.; Leijtens, T.; McGehee, M. D.; Dausardt, R. H. Cross-linkable, solvent-resistant fullerene contacts for robust and efficient perovskite solar cells with increased J_{SC} and V_{OC}. *ACS Appl. Mater. Interfaces*, **2016**, *8*, 25896-25904.

(44) Sandoval-Torrientes, R.; Pascual, J.; Garíca-Benito, I.; Collavini, S.; Kosta, I.; Tena-Zaera, R.; Martín, N.; Delgado, J. L. Modified fullerenes for efficient electron transport layer-free perovskite/fullerene blend-based solar cells. *ChemSusChem* **2017**, *10*, 2023-2029.

(45) Ruoff, R. S.; Tse, D. S.; Malhotra, R.; Lorents, D. C. Solubility of fullerene (C_{60}) in a variety of solvents. *J. Phys. Chem.* **1993**, *97*, 3379-3383.

(46) Makowski, M.; Czaplewski, C.; Liwo, A.; Scheraga, H. A. Potential of mean force of association of large hydrophobic particles: toward the nanoscale limit. *J. Phys. Chem. B* **2010**, 114, 993-1003.

(47) Zangi, R. Are buckyballs hydrophobic?. *J. Phys, Chem. B* **2014**, *118*, 12263-12270.

(48) Nakamura, J.; Nakayama, T.; Watanabe, S.; Aono, M. Structural and cohesive properties of a C_{60} monolayer. *Phys. Rev. Lett.* **2001**, *87*, 048301.

(49) Nápoles-durate, J. M.; Reyes-Reyes, M.; Ricardo-Chavez, J. L.; Garibay-Alonso, R.; López-Sandoval, R. Effect of packing on the cohesive and electronic properties of methanofullerene crystals. *Phy. Rev. B* **2008**, *78*, 035425.

(50) Lin, H.-S.; Jeon, I.; Xiang, R.; Seo, S.; Lee, J.-W.; Li, C.; Pal, A.; Manzhos, S.; Goorsky, M. S.; Yang, Y.; Maruyama, S.; Matsuo, Y. Achieving high efficiency in solution-processed perovskite solar cells using C_{60}/C_{70} mixed fullerenes. *ACS Appl. Mater. Interfaces* **2018**, *10*, 39590-39598.

(51) Santo, Y.; Jeon, I.; Yeo, K. S.; Nakagawa, T.; Matsuo, Y. Mixture of [60] and [70]PCBM giving morphological stability in organic solar cells. *Appl. Phys. Lett.* **2013**, *103*, 073306.

(52) Shin, Y.-C.; Wang, L.; Hsieh, H.-C.; Lin, K.-F. Effect of fullerene passivation on the charging and discharging behavior of perovskite solar cells: reduction of bound charges and ion accumulation. *ACS Appl. Mater. Interfaces* **2018**, *10*, 11722-11731.
(53) Fang, Y.; Bi, C.; Wang, D.; Huang, J. The functions of fullerenes in hybrid perovskite solar cells. *ACS Energy Lett.* **2017**, *2*, 782-794.
(54) Kobin, B.; Bianchi, F.; Halm, S.; Leistner, J.; Blumstengel, S.; Henneberger, F.; Hecht, S. Green emission in ladder-type quarterphenyl: beyond the fluorenone-defect. *Adv. Funct. Mater.* **2014**, *24*, 7717-7727.
(55) Dai, Y.; Feng, X.; Liu, H.; Jiang, H.; Bao, M. Synthesis of 2-naphthols via carbonylative stille coupling reaction of 2-bromobenzyl bromides with tributylallylstannane followed by the heck reaction. *J. Org. Chem.* **2011**, *76*, 10068-10077.
(56) Carpino, L. A.; Lin, Y. Z. Benz[f]indene. *J. Org. Chem.* **1990**, *55*, 247-250. (d) Reich, H. J.; Goldenberg, W. S.; Sanders, A. W.; Jantzi, K. L.; Tzschucke, C. C. Amine- and ether-chelated aryllithium reagents structure and dynamics. *J. Am. Chem. Soc.* **2003**, *125*, 3509-3521.
(57) Kohn, W.; Sham, L. Self-consistent equations including exchange and correlation effects. *J. Phy. Rev.* **1965**, *140*, A1133.
(58) Rose, A. Space-charge-limited currents in solids. *Phys. Rev.* **1955**, *97*, 1538.
(59) Han, Q.; Bae, S.-H.; Sun, P.; Hsieh, Y.-T.; Yang, Y. (Michael), Rim, Y. S.; Zhao, H.; Chen, Q.; Shi, W.; Li, G.; Yang, Y. Single crystal formamidinium lead iodide ($FAPbI_3$): insight into the structural, optical, and electrical properties. *Adv. Mater.* **2016**, *28*, 2253-2258.
(60) Min, H.; Kim, G.; Paik, M. J.; Lee, S.; Yang, W. S.; Jung, M.; Seok, S. I. Stabilization of precursor solution and perovskite layer by addition of sulfur. *Adv. Energy Mater.* **2019**, *9*, 1803476.
(61) Son, D.-Y.; Kim, S.-G.; Seo, J.-Y.; Lee, S.-H.; Shin, H.; Lee, D.; Park, N.-G. Universal approach toward hysteresis-free perovskite solar cell via defect engineering. *J. Am. Chem. Soc.* **2018**, *140*, 1358-1364.
(62) Matsuo, Y.; Iwashita, A.; Abe, Y.; Li, C.-Z.; Matsuo, K.; Hashiguchi, M.; Nakamura, E. Regioselective synthesis of 1,4-di(organo)[60]fullerenes through DMF-assisted monoaddition of silylmethyl grignard reagents and subsequent alkylation reaction. *J. Am. Chem. Soc.* **2008**, *130*, 15429-15436.
(63) Su, Y.-T.; Wang, Y.-L.; Wang, G.-W. Palladium-catalyzed heteroannulation of [60]fullerene with *N*-(2-arylethyl) sulfonamides *via* C–H bond activation. *Org. Chem. Front.* **2014**, *1*, 689-693.
(64) Zhou, D.-B.; Wang, G.-W. Synthesis of [60]fullerene-fused tetralones via palladium-catalyzed ketone-directed sp^2 C–H activation and sp^3 C–H functionalization. *Adv. Synth. Catal.* **2016**, *358*, 1548-1554.
(65) Gao, K.; Li, L.; Lai, T.; Xiao, L.; Huang, Y.; Huang, F.; Peng, J.; Cao, Y.; Liu, F.; Russell, T. P.; Janssen, R. A. J.; Peng, X. Deep absorbing porphyrin small molecule for high-performance organic solar cells with very low energy losses. *J. Am. Chem. Soc.* **2015**, *137*, 7282-7285.
(66) Cuesta, V.; Vartanian, M.; Cruz, P. d. l.; Singhal, R.; Sharma, G. D.; Langa, F. Comparative study on the photovoltaic characteristics of A–D–A and D–A–D molecules based on Zn-porphyrin; a D–A–D molecule with over 8.0% efficiency. *J. Mater. Chem. A* **2017**, *5*, 1057-1065.
(67) Tian, C.-B.; Castro, E.; Betancourt-Solis, G.; Nan, Z.-A.; Fernandez-Delgado, O.; Jankuru, S.; Echegoyen, L. Fullerene derivative with a branched alkyl chain exhibits enhanced charge extraction and stability in inverted planar perovskite solar cells. *New, J. Chem.* **2018**, *42*, 2896-2902.
(68) Azimi, H.; Ameri, T.; Zhang, H.; Hou, Y.; Quiroz, C. O. R.; Min, J.; Hu, M.; Zhang, Z.-G.; Przybilla, T.; Matt, G. J.; Spiecker, E.; Li, Y.; Brabec, C. J. A Universal interface layer based on an amine-functionalized fullerene derivative with dual functionality for efficient solution processed organic and perovskite solar cells. *Adv. Energy Mater.* **2015**, *5*, 1401692.
(69) Wang, H.; Cai, F.; Zhang, M.; Wang, P.; Yao, J.; Gurney, R. S.; Li, F.; Liu, D.; Wang, T. Halogen-substituted fullerene derivatives for interface engineering of perovskite solar cells. *J. Mater. Chem. A* **2018**, *6*, 21368-21378.
(70) Seo, S.; Jeon, I.; Xiang, R.; Lee, C.; Zhang, H.; Tanaka, T.; Lee, J.-W.; Suh, D.; Ogamoto, T.; Nishikubo, R.; Saeki, A.; Chiashi, S.; Shiomi, J.; Kataura, H.; Lee, H. M.; Yang, Y.; Matsuo, Y.; Maruyama, S. Semiconducting carbon nanotubes as crystal growth templates and grain bridges in perovskite solar cells. *J. Mater. Chem. A* **2019**, *7*, 12987-12992.
(71) Lee, J.-W.; Kim, S.-G.; Bae, S.-H.; Lee, D.-K.; Lin, O.; Yang, Y.; Park, N.-G. The interplay between trap density and hysteresis in planar heterojunction perovskite solar cells. *Nano Lett.* **2017**, *17*, 4270-4276.
(72) Hall, B. D.; Zanchet, D.; Ugarte, D. Estimating nanoparticle size from diffraction measurements. *J. Appl. Crystallogr.* **2000**, *33*, 1335-1341.
(73) Yin, J.; Cortecchia, D.; Krishna, A.; Chen, S.; Mathews, N.; Grimsdale, A. C.; Soci, C. Interfacial charge transfer anisotropy in polycrystalline lead iodide perovskite films. *J. Phys. Chem. Lett.* **2015**, *6*, 1396-1402.
(74) Wang, Q.; Lyu, M.; Zhang, M.; Yun, J.-H.; Chen, H.; Wang, L. Transition from the tetragonal to cubic phase of organohalide perovskite: the role of chlorine in crystal formation of $CH_3NH_3PbI_3$ on TiO_2 substrates. *J. Phys. Chem. Lett.* **2015**, *6*, 4379-4384.
(75) Li, Z.; Kolodziej, C.; McCleese, C.; Wang, L.; Kovalsky, A.; Samia, A. C.; Zhao, Y.; Burda, C. Effect of chloride substitution on interfacial charge transfer processes in $MAPbI_3$ perovskite thin film solar cells: planar versus mesoporous. *Nanoscale Adv.* **2019**, *1*, 827-833.
(76) Liu, C.; Wang, K. Du, P.; Meng, T.; Yu, X.; Cheng, S. Z. D.; Gong, X. High performance planar heterojunction perovskite solar cells with fullerene derivatives as the electron transport layer. *ACS Appl. Mater. Interfaces* **2015**, *7*, 1153-1159.
(77) Tao, C.; Velden, J. V. D.; Cabau, L.; Montcada, N. F.; Neutzner, S.; Kandada, A. R. S.; Marras, S.; Brambilla, L.; Tommasini, M.; Xu, W.; Sorrentino, R.; Perinot, A.; Caironi, M.; Bertarelli, C.; Palomares, E.; Petrozza, A. Fully solution-processed n-i-p-like perovskite solar cells with planar junction: how the charge extracting layer determines the open-circuit voltage. *Adv. Mater.* **2017**, *29*, 1604493.
(78) Zhou, W.; Zhen, J.; Liu, Q.; Fang, Z.; Li, D.; Zhou, P.; Chen, T.; Yang, S. Successive surface engineering of TiO_2 compact layers *via* dual modification of fullerene derivatives affording hysteresis-suppressed high-performance perovskite solar cells. *J. Mater. Chem. A* **2017**, *5*, 1724-1733.
(79) Y.-C. Wang, X. Li, L. Zhu, X. Liu, W. Zhang and J. Fang, Efficient and hysteresis-free perovskite solar cells based on a solution processable polar fullerene electron transport layer. *Adv. Energy Mater.* **2017**, *7*, 1701144.
(80) Wojciechowski, K.; Ramirez, I.; Gorisse, T.; Dautel, O.; Dasari, R.; Sakai, N.; Hardigree, J. M.; Song, S.; Marder, S.; Riede, M.; Wantz, G.; Snaith, H. J. Cross-linkable fullerene derivatives for solution-processed n-i-p perovskite solar cells. *ACS Energy Lett.* **2016**, *1*, 648-653.
(81) Dong, Y.; Li, W.; Zhang, X.; Xu, Q.; Liu, Q.; Li, C.; Bo, Z. Highly efficient planar perovskite solar cells via interfacial modification with fullerene derivatives. *Small* **2016**, *12*, 1098-1104.
(82) Xu, Q.; Lu, Z.; Zhu, L.; Kou, C.; Liu, Y.; Li, C.; Meng, Q.; Li, W.; Bo, Z. Elimination of the J–V hysteresis of planar perovskite solar cells by interfacial modification with a thermo-cleavable fullerene derivative. *J. Mater. Chem. A* **2016**, *4*, 17649-17654.
(83) McMeekin, D. P.; Sadoughi, G.; Rehman, W.; Eperon, G. E.; Saliba, M.; Hörantner, M. T.; Haghighirad, A.; Sakai1, N.; Korte, L.; Rech, B.; Johnston, M. B.; Herz1, L. M.; Snaith, H. J. A mixed-cation lead mixed-halide perovskite absorber for tandem solar cells. *Science* **2016**, *351*, 151-155.
(84) Zhang, Y.; Wang, P.; Yu, X.; Xie, J.; Sun, X.; Wang, H.; Huang, J.; Xu, L.; Cui, C.; Lei, M.; Yang, D. Enhanced performance and light soaking stability of planar perovskite solar cells using an amine-based fullerene interfacial modifier. *J. Mater. Chem. A* **2016**, *4*, 18509-18515.
(85) Cao, T.; Wang, Z.; Xia, Y.; Song, B.; Zhou, Y.; Chen, N.; Li, Y. Facilitating electron transportation in perovskite solar cells via water-soluble fullerenol interlayers. *ACS Appl. Mater. Interfaces* **2016**, *8*, 18284-18291.
(86) Ryu, S.; Seo, J.; Shin, S. S.; Kim, Y. C.; Jeon, N. J.; Noh, J. H.; Seok, S. I. Fabrication of metal-oxide-free $CH_3NH_3PbI_3$ perovskite solar cells processed at low temperature. *J. Mater. Chem. A* **2015**, *3*, 3271-3275.
(87) Ke, W.; Zhao, D.; Grice, C. R.; Cimaroli, A. J.; Ge, J.; Tao, H.; Lei, H.; Fang, G.; Yan, Y. Efficient planar perovskite solar cells using room-temperature vacuum-processed C_{60} electron selective layers. *J. Mater. Chem. A* **2015**, *3*, 17971-17976.

Highly selective and scalable fullerene-cation-mediated synthesis accessing cyclo[60]fullerenes with 5-membered-carbon-ring and their application to perovskite solar cells